Published in final edited form as:
ACS Nano. 2012 May 22; 6(5): 3695–3702. doi:10.1021/nn301218z.

Ag_2S Quantum Dot: A Bright and Biocompatible Fluorescent Nanoprobe in the Second Near-Infrared Window

Yan Zhang[1,$], **Guosong Hong**[2,$], **Yejun Zhang**[1,$], **Guangcun Chen**[1], **Feng Li**[1], **Hongjie Dai**[2,*], and **Qiangbin Wang**[1,*]

[1]Division of Nanobiomedicine and *i*-Lab, Suzhou Institute of Nano-Tech and Nano-Bionics, Chinese Academy of Sciences, Suzhou 215123, P. R. China

[2]Department of Chemistry, Stanford University, Stanford, CA 94305-5080 USA

Abstract

Ag_2S quantum dots (QDs) emitting in the second near-infrared region (NIR-II, 1.0~1.4 μm) are demonstrated as a promising fluorescent probe with both bright photoluminescence and high biocompatibility for the first time. Highly selective *in vitro* targeting and imaging of different cell lines are achieved using biocompatible NIR-II Ag_2S QDs with different targeting ligands. The cytotoxicity study illustrates the Ag_2S QDs with negligible effects in altering cell proliferation, triggering apoptosis and necrosis, generating reactive oxygen species (ROS), and causing DNA damage. Our results have opened up the possibilities of using these biocompatible Ag_2S QDs for *in vivo* anatomical imaging and early-stage tumor diagnosis with deep tissue penetration, high sensitivity, as well as elevated spatial and temporal resolution owing to their high emission efficiency in the unique NIR-II imaging window.

Keywords

Ag_2S quantum dot; near-infrared; cytotoxicity; cellular imaging; biocompatibility

Fluorescent imaging in the second near-infrared window (NIR-II, 1.0~1.4 μm) is appealing due to minimal autofluorescence and negligible tissue scattering in this region, affording maximal penetration depth for deep tissue imaging with high feature fidelity.[1–4] Simulations and modeling studies suggested that fluorophores with emission in the 1000 – 1320 nm NIR-II region could significantly improve signal-to-noise ratio compared to those emitting at 750~850 nm (NIR-I).[5] Recent efforts have been devoted to identifying NIR-II emitting agents for *in vivo* imaging applications. Quantum dots (QDs) such as PbSe[6], PbS[7], and CdHgTe[8] with NIR emission have been successfully developed. However, the highly toxic nature of Pb, Cd and Hg is of concern for *in vivo* applications.[9] Therefore, highly biocompatible NIR-II fluorescent probes that do not contain Cd, Pd or Hg will facilitate biological imaging in this beneficial spectral region.[9–17]

Recently, single-walled carbon nanotubes (SWNTs) have been demonstrated as promising candidates for biological imaging and sensing with unique fluorescence in the NIR-II

*To whom correspondence should be addressed. qbwang2008@sinano.ac.cn; hdai1@stanford.edu.
$These authors contributed equally to this work.

Supporting Information Available: Additional details of the photostability measurement of Ag_2S QDs, the dynamic light scattering and zeta potential measurement of DHLA-Ag_2S QDs and PEGylated-DHLA-Ag_2S QDs, the long time *in situ* imaging of QD-RGD stained U87 MG cells, the cytotoxicity studies of DHLA-Ag_2S on the U87 MG cells, the effects of MPA-CdSe@ZnS QDs on the cell proliferation and comet assay of U87 MG and L929 cells, and the TEM images of L929 cellular uptake of Ag_2S are included. This material is available free of charge *via* the Internet at http://pubs.acs.org.

region.[1–3,10–12] The Dai group has shown that SWNTs can be used as sensitive NIR-II fluorescence probes for imaging both *in vitro* and in live mice.[1–3,13–17] High imaging contrast was achieved at a relatively low dose (3.4 μg) for whole-body mouse imaging as well as intravital small vessel imaging inside tumors on tumor-bearing mice.[1] Furthermore, real-time video rate imaging of SWNT circulation through different mouse organs, including the lungs, kidneys, spleen, liver and pancreas, can be clearly observed for detailed anatomical information during intravenous injection of SWNTs.[2] However, a pitfall is that the fluorescence quantum yield (QY) of SWNTs is relatively low, a few percent at the best.[18,19] There is an urgent need to develop brighter fluorophores in the NIR-II window for imaging in this beneficial region.

More recently, we first reported a new type of NIR QDs, Ag_2S QDs, with emission in the NIR-II region.[20,21] Ag_2S QDs should be more biocompatible owing to the absence of any toxic metals such as Cd, Pb, and Hg. In addition, Ag_2S exhibits an ultralow solubility product constant ($K_{sp} = 6.3 \times 10^{-50}$), which ensures the minimum amount of Ag ion released into the biological surroundings. In this work, for the first time, molecular imaging of live cells with Ag_2S QDs as an NIR-II probe was achieved and the cytotoxicity of Ag_2S QDs was comprehensively studied. These results demonstrated that Ag_2S QD is an attractive NIR-II fluorescence nanoprobe with high quantum efficiency and decent biocompatibility.

RESULTS AND DISCUSSION

Ag_2S QDs were prepared according to our previous reports[20,21] with some modifications. In a typical reaction, 0.1 mmol of $(C_2H_5)_2NCS_2Ag$ was added into 10 g of 1-dodecanethiol (DT) in a three-necked flask (100 mL) at room temperature. The slurry was vacuumed for 5 min to remove oxygen under vigorous magnetic stirring. The solution was then heated to 210 °C at a heating rate of 15 °C/min and kept for 1 h under N_2 atmosphere. Hydrophobic Ag_2S QDs with an average diameter of 5.4 nm coated with DT as the surface ligand were obtained. It was noticeable that the Ag_2S QDs obtained by merely using DT as both covalent ligand and solvent afforded the brightest photoluminescence (PL), in comparison to previous reports[20,21]. More importantly, we observed an interesting phenomenon that the emission of Ag_2S QDs did not depend on the size. As shown in Figure 1, three samples of Ag_2S QDs with different sizes of 5.4 nm, 7 nm and 10 nm exhibited similar NIR spectra with identical peak position, except for the decrease of PL intensity as particle sizes increased. The 5.4 nm-sized Ag_2S QDs were used for all the following experiments of cell staining and cytotoxicity assessment.

To rationalize the unusual size-independent emission of Ag_2S QDs, we proposed that it was the DT molecules that played a key role in determining the optical properties of Ag_2S. In our previous report,[20] Ag_2S QDs were synthesized by pyrolysis of $(C_2H_5)_2NCS_2Ag$ in a mixture of oleic acid, octadecylamine and 1-octadecane, where an extraordinarily narrow full width at half maximum (FWHM) of 21 nm with emission peak at 1058 nm was found for Ag_2S QDs with oleic acid and octadecylamine as surface capping ligands.[20] Instead, the Ag_2S QDs obtained in this study were prepared through thermal decomposition of $(C_2H_5)_2NCS_2Ag$ with DT as covalent ligand and solvent and were exclusively coated with DT molecules, which might be involved in the reaction as partial sulfur source and the only capping ligand. This different recipe for making the Ag_2S QDs resulted in this new observation. Nevertheless, full understanding of this mechanism is still under investigation.

Ligand-exchange of DT with dihydrolipoic acid (DHLA) was processed to render Ag_2S QDs hydrophilic with carboxylic acid group for further biomolecular conjugation. Ag_2S QDs stayed monodisperse with narrow size distribution and considerable stability before and after the ligand exchange process (Figure 2A and 2B; Figure S1 and S2). Their average

diameter was 5.4 ± 0.3 nm, based on statistical analysis of ~100 nanoparticles. Figure 2C exhibited the PL spectra of the as-prepared DT-Ag_2S QDs and DHLA-Ag_2S QDs under the excitation of a 658 nm laser diode. A 30-nm red shift in the PL peak position and a 43-nm widened FWHM were observed in the spectrum of DHLA-Ag_2S QDs compared to that of DT-Ag_2S QDs, which could be attributed to the change of refractive index of the coating layer. A PL image taken in the 1100 – 1700 nm spectral range was shown in Figure 2C for the DHLA-Ag_2S QDs excited by an 808 nm laser (power density: 0.25 W/cm^2, exposure time: 10 ms), which exhibited the bright fluorescence of DHLA-Ag_2S QDs. The QY of DHLA-Ag_2S QDs was characterized to be 5.8%, with an NIR standard dye IR-26 as the reference (QY = 0.5%).[22] Poly(ethylene glycol) (PEG) was further used to encapsulate and stabilize the DHLA-Ag_2S QDs *via* ethyl (dimethylaminopropyl) carbodiimide/N-hydroxy-succinimide (EDC/ NHS) chemistry between the –COOH groups of DHLA and –NH_2 groups of amine functionalized six-armed PEG. The PEGylated-DHLA-Ag_2S QDs were measured to retain higher QY of 15.5%, which could be attributed to better encapsulation and protection of PEG on the Ag_2S surfaces than DHLA only. As expected, the negatively charged DHLA-Ag_2S QDs became neutral after PEGylation (Figure S3 and S4). In comparison to SWNTs, DHLA-Ag_2S QDs and PEGylated-DHLA-Ag_2S QDs were 2.1 times and 5.6 times brighter than the reported cholate-suspended SWNTs[1].

To demonstrate the feasibility of these bright Ag_2S QDs as effective NIR-II emissive probes, targeted cell imaging was carried out in the 1100 - 1700 nm range using the intrinsic NIR-II fluorescence of the DHLA-Ag_2S QDs (Figure 3). Two cell lines, human breast cancer cell line (MDA-MB-468) and human glioblastoma cell line (U87 MG), were specifically chosen for cell targeting experiment, since they represented two cell types with very different levels of expression of two membrane receptors, epidermal growth factor receptor (EGFR) and $\alpha_v\beta_3$ integrin. Cetuximab (Erbitux®) protein and cyclic arginine-glycine-aspartic acid (RGD) peptide were selected for their specific targeting to EGFR and $\alpha_v\beta_3$ integrin,[1,23] respectively, and they were conjugated to the carboxyl groups of DHLA ligands on Ag_2S QD surfaces *via* the EDC/NHS coupling chemistry. All cell staining experiments with Ag_2S QDs were conducted in phosphate buffered saline (PBS) at 4 °C for 2 h. The EGFR-positive MDA-MB-468 cell line treated with the DHLA-Ag_2S QD/Erbitux conjugate (Figure 3A) showed high NIR PL signals (red-white), whereas the EGFR-negative U87 MG cell line (Figure 3C) showed very little signal. Furthermore, the $\alpha_v\beta_3$-positive U87 MG cell line treated with the DHLA-Ag_2S QD/RGD conjugate (Figure 3G) also showed high NIR PL signals (red-white), whereas the $\alpha_v\beta_3$-negative MDA-MB-468 cell line (Fig. 3E) did not. As an additional negative control, the labeling experiment was executed with the uncoated DHLA-Ag_2S QDs, and very little NIR-II fluorescence was observed for both cell lines (Figure S5). These observations demonstrated that (1) Ag_2S QDs can be used for selective cell targeting and imaging as a new type of NIR-II nanoprobe with high PL intensity; and (2) Ag_2S QDs can be functionalized to obtain either biologically active or inert surface coatings for specific targets.

It is worth noting that both the DHLA-Ag_2S QD/Erbitux conjugates and DHLA-Ag_2S QD/ RGD conjugates were incubated with the MDA-MB-468 cells and U87 MG cells at 4 °C. Such a low temperature blocked the endocytosis of Ag_2S QDs and avoided any non-specific active cell uptake of Ag_2S QDs.[14,24] The Ag_2S QDs were simply bound to the cell membrane receptors through the specific recognition of the ligands conjugated on the QD surfaces and thus truly reflected the level of membrane receptor expression. As a result, 4 °C incubation helped improve the specificity of cell staining since higher temperature would have caused non-specific uptake by the negative cell lines. As for the round shape of the cellular morphology shown in the white light optical images in Figure 3, it was due to the shape changes induced by trypsinization before cell staining, and not from the cell damage caused by Ag_2S QDs. The reason for using trypsinized, round-shaped cells instead of

adherent cells was the size of Ag_2S QDs used here for staining. Unlike small molecules such as membrane staining dyes that could perfuse freely on the membrane, QDs had difficulties to access the bottom contact area of adherent cells for obtaining uniform staining on the cell membrane. Cells had to be detached from the culture substrate to afford the maximum accessible surface area with enough exposed receptors for conjugated QDs to bind to. After staining at 4 °C, the Ag_2S QD-labeled U87-MG cells as shown in Figure 3G were incubated at 37 °C, and the low-temperature-induced shape change was observed to be gradually reversed,[25] as shown in Figure S7. Figure S7 also illustrated the Ag_2S QDs with high physical stability and retained PL intensity over 4 h incubation with cells, which further supported the possible *in vitro/in vivo* applications of Ag_2S QDs in the future.

Although Ag_2S QDs have shown their promise as a new type of NIR-II probe, their biocompatibility is critical for their potential *in vitro* applications. Hence, we systematically studied the cytotoxicity of Ag_2S QDs, including cell proliferation, cell apoptosis/necrosis, production of reactive oxygen species (ROS), and comet test for DNA damage detection, to examine the biocompatibility of Ag_2S QDs *in vitro*. Mouse fibroblast L929 cell line was chosen for the cytotoxicity study. Since our goal was to study how the Ag_2S QDs would affect the cellular behaviors in general, L929 cells without over-expressed or under-expressed receptors will be more objective in assessing the cytotoxicity of Ag_2S QDs, instead of U87 MG or MDA-MB-468 cell lines with over-expressed membrane receptors.

Cell proliferation reflects an increase in cell numbers as the result of cell growth and division, which is a fundamental method for assessing the impact of toxicant on cell health and genotoxicity. Figure 4 shows the proliferation of L929 cells after 72 h exposure to five different concentrations: 6.25 μg/mL, 12.5 μg/mL, 25 μg/mL, 50 μg/mL, and 100 μg/mL of Ag_2S QDs. It was observed that the cell proliferation was dose-independent, where both the total number of cells (stained with Hoechst) and the number of cells with newly synthesized DNA (stained with EdU) presented no statistically significant difference. This observation suggested that Ag_2S QDs did not interfere with the cell proliferation, which was good for their use of *in vitro* labeling. In the meantime, the effects of PEGylated-DHLA-Ag_2S QDs and the popular 3-mercaptopropionic acid (MPA)-capped CdSe@ZnS QDs on L929 cell proliferation were further studied as references. As shown in Figure 4, there is no statistical difference of the cell proliferation performance between the DHLA-Ag_2S QDs and PEGylated-DHLA-Ag_2S QDs. However, the proliferation of L929 cells was severely disturbed with the CdSe@ZnS QDs. These observations illustrated that the biocompatible nature of Ag_2S without side effect on the cell proliferation.

Annexin V-FITC staining and propidium iodide (PI) incorporation were performed to study the cell apoptosis and cell necrosis induced by Ag_2S QDs. The flow cytometry data as shown in Figure 5 demonstrated that the Ag_2S QDs had negligible cytotoxicity in terms of induced apoptosis and necrosis on L929 cells after 72 h treatment. In the fluorescence activated cell sorting (FACS) dot plot, each dot represented an individual cell. The cells appearing in the lower left quadrant (Q3) stood for the normal cells, and the cells appearing in the upper left quadrant (Q1) denoted the necrosis cells. While those appearing in the upper right quadrant (Q4) and lower right quadrant (Q2) represented the cells in the early and late apoptotic stages, respectively. With the concentration of Ag_2S QDs at 6.25 μg/mL, 12.5 μg/mL, 25 μg/mL, 50 μg/mL, and 100 μg/mL, the populations of L929 cells that underwent apoptosis and necrosis remained constant without statistically significant difference in comparison to those of the control experiment without Ag_2S QDs. These results illustrated the high biocompatible nature of the DHLA-Ag_2S QDs.

Oxidative stress is usually defined as an index of redox imbalance in cells resulting from the increased intracellular ROS.[26] The formation of ROS induced by addition of DHLA-Ag_2S

QDs was measured *via* monitoring the fluorescence intensity of 2', 7'-dichlorofluorescein (DCF). The ROS assay employed the cell-permeable fluorogenic probe DCFH-DA which diffused into cells and was hydrolyzed by cellular esterase into the non-fluorescent DCFH. In the presence of ROS, DCFH is rapidly oxidized to highly fluorescent DCF. The flow cytometry results (Figure 6) demonstrated that L929 cells treated with Ag_2S QDs in a wide range of 6.25 to 100 μg/mL for 72 h produced negligible amount of ROS, which had no statistically significant difference in comparison to that of the negative control (0 μg/mL). It has been well documented that the formation of ROS caused by the presence of nanoparticles is considered to be the major cause of spontaneous damage to DNA, followed by the cell apoptosis and necrosis.[27] Taking into account both apoptosis/necrosis and ROS results, we believed that Ag_2S QDs was highly biocompatible since both the apoptosis/necrosis and ROS results presented negligible toxicity of Ag_2S QDs at concentrations up to 100 μg/mL.

To gain further understanding of the biocompatibility of Ag_2S QDs, we conducted the single-cell gel electrophoresis assay (comet assay) to detect the genotoxicity induced by Ag_2S QDs. Comet assay has been considered as a well-established, simple, versatile, and sensitive tool to quantitatively assess DNA damage in individual cell populations.[28] The head is composed of intact DNA, while the tail consists of damaged or broken pieces of DNA. The brighter and longer the tail is, the higher the level of damage. As shown in Figure 7, there were no statistically significant differences in both tail length and tail moment when L929 cells were treated with Ag_2S QDs in a series of concentrations ranging from 0, to 6.25, 12.5, 25, 50, 100 μg/mL for 72 h, respectively. The percentage of DNA content in the comet tail also did not show notable changes when the Ag_2S QDs concentration was raised, which is consistent with the results of DNA tail length and tail moment. These results illustrated the Ag_2S QDs with negligible genotoxicity.

CONCLUSION

In summary, we have demonstrated that Ag_2S QDs can be used as a promising NIR-II probe with both bright photoluminescence and high biocompatibility. Through the bioconjugation of Ag_2S QDs with specific ligands, targeted labeling and imaging of different cell lines were achieved. The cytotoxicity study has illustrated the Ag_2S QDs with negligible toxicity in terms of cell proliferation, apoptosis and necrosis, ROS, and DNA damage. We envisage this new type of NIR-II QDs with great potential in *in vivo* anatomical imaging, disease detection and cancer diagnosis, where a systematic investigation of the *in vivo* biodistribution, degradation, and clearance of the Ag_2S QDs in addition to their *in vivo* imaging capabilities is needed and currently under way.

METHODS

Chemicals and cell lines

For purpose of surface functionalization, the following chemicals were used: 1-dodecanethiol (DT, 98%, aladdin), dihydrolipoic acid (DHLA, 98%, Alfa Aesar), poly(ethylene glycol) (PEG, 90%, SunBio), ethyl (dimethylaminopropyl) carbodiimide (EDC, commercial grade, Sigma), N-hydroxy-succinimide (NHS, 98.5%, Sigma). Other chemicals including $AgNO_3$ (AR), dimethyl sulfoxide (DMSO, AR), $(C_2H_5)_2NCS_2Na{\cdot}3H_2O$ (Na(DDTC)), ethanol (AR), and cyclohexane (AR) were purchased from Sinopharm Chemical Reagent Company. All chemicals were used as received without further purification. Biological materials used in this study are listed as follows: Mouse fibroblast L929 cell line (The Cell Bank of Type Culture Collection of Chinese Academy of Sciences), human malignant glioma U87 MG cell line (The Cell Bank of Type Culture Collection of Chinese Academy of Sciences), human breast cancer MDA-MB-468 cell line

(ATCC), Erbitux (DrugBank), cyclo-RGDfK (cyclic arginine-glycine-aspartic acid, Biomol). CdSe@ZnS QD530 powder was purchased from Ocean NanoTech. Water solubilization with mercaptopropionic acid (MPA) and concentration determination were carried out using reported methods[29].

Preparation of $(C_2H_5)_2NCS_2Ag$

In a typical synthesis, 0.1 mol of $AgNO_3$ and $(C_2H_5)_2NCS_2Na{\cdot}3H_2O$ were firstly dissolved in 80 mL of distilled water, respectively. Then, the two solutions were mixed with stirring in a 200 mL beaker. After sitting at constant ambient condition for 2 h, the resultant yellow precipitate was filtered, washed with distilled water, and dried in air at 60 °C.

Synthesis of hydrophobic Ag_2S QDs with different size distributions

A typical procedure is described as follows: a given amount of Ag(DDTC) (0.1 mmol) was added into 10 g DT in a three-necked flask (100 mL) at room temperature. Then, oxygen was removed from the slurry with vigorous magnetic stirring under vacuum for 5 min. The solution was heated to different temperatures including 210 °C and 230 °C at a heating rate of 15 °C/min and kept at a constant temperature for 1 h under N_2 atmosphere. Then it was allowed to cool down to room temperature naturally. Subsequently 50 mL of ethanol was poured into the solution, and the resultant mixture was centrifugally separated with a centrifugal force of 6729 g for 20 min and the products were collected. Note that 210 °C resulted in Ag_2S QDs with an average size of 5.4 nm, and 230 °C gave 7 nm-sized Ag_2S QDs. For the synthesis of 10 nm Ag_2S QDs, its procedure is same to that of 5.4 nm-sized Ag_2S QDs except the employed silver source $AgNO_3$ (0.1 mmol).

Preparation of hydrophilic Ag_2S QDs

A mixture of as-prepared Ag_2S sample (0.05 mmol), cyclohexane (15 mL), ethanol (15 mL) and DHLA (0.15 g) were stirred at room temperature for 48 h. The product was then isolated by centrifugation with a centrifugal force of 26916 g for 20 min, washed with deionized water, and re-dispersed in deionized water. The pH of the solution was adjusted to 7.2 by adding NH_4OH solution. The DHLA-Ag_2S QDs with carboxylic acid groups on the surface were ready for conjugation with biomolecules *via* EDC/NHS chemistry.

Characterizations

The sizes of as-prepared Ag_2S QDs were examined by a Tecnai G2 F20 S-Twin transmission electron microscopy (TEM, FEI, USA) operated at 200 kV. The absorption spectra of Ag_2S QDs were recorded with a Perkin Elmer Lambda 25 UV-Vis spectrometer. The NIR-II fluorescence spectra of Ag_2S QDs were collected on an Applied NanoFluorescence Spectrometer (USA) at room temperature with an excitation laser source of 658 nm. The hydrodynamic sizes and size distributions, as well as the zeta potentials of the Ag_2S QDs were measured using a Malvern Nanosizer.

Conjugation of DHLA-Ag_2S QD with Erbitux and RGD

0.1 mg of Ag_2S QDs was first dissolved in 200 μL of DMSO, and then 1.15 mg (0.01mmol) of NHS dissolved in 50 μL of DMSO was added into QD solution while keeping stirring. 1.91 mg (0.01mmol) of EDC was dissolved in 50 μL of DMSO and was added into the QD-NHS/DMSO solution. Reaction was allowed to last for 1 h in dark with stirring. The surface activated Ag_2S QDs were centrifuged and washed with DMSO for twice and further dispersed in DMSO solution. 2×10^{-9} mol of Erbitux protein and 2×10^{-9} mol of cyclo-RGDfK (RGD-lysine) in PBS buffer were then conjugated with the EDC/NHS-activated DHLA-Ag_2S QDs, respectively. The conjugated products of ~100 μg/mL were further used for staining trypsinized MDA-MB-468 cells (positive to Erbitux and negative to RGD) and

U87 MG cells (positive to RGD and negative to Erbitux) for 2 h at 4 °C. Labeled cells were washed three times using 1× PBS to remove unbound QDs.

High magnification NIR-II photoluminescence cell imaging

5 μL of stained U87-MG or MDA-MB-468 cell suspension was transferred to 200 μL of 1× PBS, placed into an 8-well chamber slide (Lab-Tek™ Chambered Coverglass, 1.0 Borosilicate). The chamber slide was kept in a temperature controlled chamber (BC-260W, 20/20 Technology, Inc.) for epifluorescence imaging. Temperature was kept at 4 ºC by heat exchanger (HEC-400, 20/20 Technology, Inc.), and the CO_2 gas flow was kept at 1 L/min by a gas purging system (GP-502, 20/20 Technology, Inc.). Targeted cell imaging was done using a 658-nm laser diode excitation with an 80 μm diameter spot focused by a ×100 objective lens (Olympus). The resulting NIR-II photoluminescence was collected using a liquid-nitrogen-cooled, 320 × 256 pixel, two-dimensional InGaAs camera (Princeton Instruments) with a sensitivity ranging from 800 to 1,700 nm. The excitation light was filtered out using a 900 nm long-pass filter and an 1100 nm long-pass filter (both Thorlabs) so that the intensity of each pixel represented light in the 1,100 – 1,700 nm NIR-II range. The NIR photoluminescence images were taken at a fixed exposure time of 3 s. For bright field white light images, a fiber optic illuminator (Fiber-Lite) was used for illuminating the sample in the trans-illumination mode and the images were taken using the same filters at a fixed exposure time of 2 ms. Matlab 7 was used to process the images for any necessary flat-field correction.

Cells Culture

All culture media were supplemented with 10 % fetal bovine serum, 100 IU/mL penicillin, 100 μg/mL streptomycin. U87 MG cells were cultured in Low Glucose Dulbecco's Modified Eagle Medium (DMEM), with 1 g/L D-glucose and 110 mg/L sodium pyruvate at 37 °C, 5% CO_2. MDA-MB-468 cells were cultured in Leibovitz's L-15 medium at 37 °C, CO_2 free. L929 cells were cultured in RPMI 1640 medium at 37 °C, 5% CO_2-humidified environment. All the experiments related to cells were conducted under 80% confluency.

Cell Proliferation Assay

The effect of Ag_2S on cell proliferation was measured by 5-ethynyl-20-deoxyuridine (EdU) incorporation assay using EdU assay kit (Ribobio). Briefly, L929 cells were cultured in 96-well plates. After starvation overnight, the cells were incubated with 200 μL of 6.25 μg/mL, 12.5 μg/mL, 25 μg/mL, 50 μg/mL, and 100 μg/mL of Ag_2S QDs for 72 h at 37 °C. And then the cells were exposed to 50 μM/L of EdU (Ribobio) for additional 4 h at 37°C. The cells were fixed with 4% formaldehyde for 30 min at room temperature and treated with 0.5% Triton X-100 for 20 min at room temperature for permeabilization. After being washed with PBS for three times, the cells were allowed to react with 1× Apollo® reaction cocktail (Ribobio, 100 μL/well) for 30 min. Subsequently, the DNA contents were stained with Hoechst 33342 (5 μg/mL, 100 μL/well) for 30 min and visualized under a fluorescent microscope. The EdU positive cells (red cells) were counted using Image-Pro Plus (IPP) 6.0 software (Media Cybernetics, Bethesda, MD, USA). The EdU incorporation rate was expressed as the ratio of EdU positive cells to total Hoechst33342 positive cells (blue cells). All experiments were done in triplicate and three independent repeating experiments were performed.

Apoptosis and Necrosis Assay

L929 cells were plated into 6-well plate at a density of 2×10^5 cells per well overnight, and then treated with different concentrations of Ag_2S QDs for 72 h at 37 °C. The cells were harvested, washed twice with PBS, and incubated with anti-annexin V-fluorescein

isothiocyanate (FITC) and propidium iodide (PI). Single-cell suspensions were analyzed by FACS. 0.1 μM of acinomycin D and 1 mM of H_2O_2 were employed as the apoptosis positive control and necrosis positive control, respectively.[30]

ROS Assay

L929 cells were plated into 6-well plate at a density of 2×10^5 cells per well overnight, and then treated with different concentrations of Ag_2S QDs for 72 h at 37 °C.. Then cells were harvested, washed twice with PBS, and incubated with 1 μL of 40 μM dichlorofluorescein (DCFH-DA) diluted in PBS. After incubation at 37 °C for 30 min, cells were washed twice with PBS. In the positive control Rosup group, cells were treated with 50 μg/ml Rosup for 30 min at 37 °C, and then incubated with 1 μL of 40 μM dichlorofluorescein (DCFH-DA) diluted in PBS. After incubation at 37 °C for 30 min, cells were washed twice with PBS. The fluorescence of oxidized DCFH was measured immediately by FACS.

Alkaline Single-Cell Gel Electrophoresis (Comet Assay)

Alkaline single cell gel electrophoresis (Comet assay) detects DNA damage through electrophoresis and subsequent staining in propidium iodide (PI). L929 cells were treated with different concentrations of Ag_2S QDs for 72 h at 37 °C.. Each slide was prepared by coating with 100 μL of 0.5 % normal melting agarose and stored at 4 °C. Then, 1×10^5 cells were harvested, washed twice with PBS, resuspended with 75 μL of 0.7 % low melting agarose and added to the bottom layer agarose. Subsequently, the cells were lysed under alkaline conditions in 2.5 M NaCl, 10 mM Tris, 100 mM EDTA-Na_2 at pH 10 with 1% Triton X-100 and 10% DMSO added just prior to use for 2 h. After cell lysis, the slides were equilibrated for 60 min in a jar containing alkaline buffer (300 mM NaOH, 1 mM EDTA, pH >13; 4 °C), transferred into an electrophoresis unit with alkaline buffer, and subjected to an electric field of 0.8 V/cm and 200 mA for 20 min at 4 °C. Following electrophoresis, the microgels were neutralized in 0.4 M Tris (pH 7.5), and were stained with 2.5 μg/mL propidium iodide. Fifty cells were scored per sample. Tail length and tail DNA% were measured using casp 1.2.2. The effects of Ag_2S QDs treatment on DNA migration were analyzed with the Friedman test using the SPSS 13.0 program.

Data analysis

Statistical analysis of all data was limited to Analysis of Variance (ANOVA). The statistically significant difference was considered to be $P < 0.05$.

Long Time *in situ* Imaging

It was observed that the morphologies of our stained cells were spherical, while their natural shape should be fusiformis. This morphology change was not due to the cytotoxicity of Ag_2S QDs. It was caused by the trypsinization of cells before staining at 4 °C. To reverse the change of cellular morphology and to test the cell viability after staining at 4 ºC, the chamber temperature was increased from the initial temperature of 4 ºC and stabilized at 37 ºC. The camera then monitored the change of cell morphology and PL intensity by taking images at 2 h and 4 h. When the cells were incubated at 37 °C, the morphology changing from sphere to fusiformis was observed. This observation further illustrated the negligible cytotoxicity of Ag_2S QDs.

Transmission Electron Microscopy (TEM) of Ag_2S QDs Treated Cells

Cells were treated with 0 ug/ml, 12.5 ug/ml and 100 ug/ml Ag_2S QDs for 72 h. At the end of the incubation period, cells were washed twice by PBS to get rid of the excess Ag_2S QDs, then fixed by 2.5% glutaraldehyde for 2 h at 4 °C and scraped together. Post-fixation staining was done using 1% osmium tetroxide for 1 h at room temperature. Cells were

washed well and dehydrated in alcohol (40, 50, 70, 80, 90, 95, and 100% ethanol) and treated twice with propylene oxide for 30 min each, followed by treatment with propylene oxide, spurr's low viscosity resin (1:1), for 18 h. Cells were further treated with pure resin for 24 h and embedded in beem capsules containing pure resin. Resin blocks were hardened at 70 °C for 2 days. The sections were stained with 1% lead citrate and 0.5% uranyl acetate and analyzed under HITACHI H-7000FA.

Supplementary Material

Refer to Web version on PubMed Central for supplementary material.

Acknowledgments

Q. Wang acknowledges funding by the "Bairen Ji Hua" program and "Strategic Priority Research Program" (Grant No. XDA01030200) from CAS, MOST (Grant No. 2011CB965004), and NSFC (Grant No. 20173225); H. Dai thanks funding by NIH-National Cancer Institute Grant 5R01CA135109-02. The authors thank Prof. Z.-P. Zhang at the Core Facility Center of Wuhan Institute of Virology, CAS, for his help on TEM imaging of cellular uptake of Ag_2S, and thank S. M. Tabakman for proof reading.

References

1. Welsher K, Liu Z, Sherlock SP, Robinson JT, Chen Z, Daranciang D, Dai H. A Route to Brightly Fluorescent Carbon Nanotubes for Near-Infrared Imaging in Mice. Nat Nanotech. 2009; 4:773–780.
2. Welsher K, Sherlock SP, Dai H. Deep-Tissue Anatomical Imaging of Mice Using Carbon Nanotube Fluorophores in the Second Near-Infrared Window. PNAS. 2011; 108:8943–8948. [PubMed: 21576494]
3. Liu Z, Tabakman S, Welsher K, Dai H. Carbon Nanotubes in Biology and Medicine: *In vitro* and in vivo Detection, Imaging and Drug Delivery. Nano Res. 2009; 2:85–120. [PubMed: 20174481]
4. Smith AM, Mancini MC, Nie SM. Second Window for in vivo Imaging. Nat Nanotech. 2009; 4:710–711.
5. Lim YT, Kim S, Nakayama A, Scott NE, Bawendi M, Frangioni JV. Selection of Quantum Dot Wavelengths for Biomedical Assays and Imaging. Mol Imaging. 2003; 2:50–64. [PubMed: 12926237]
6. Wehrenberg BL, Wang C, Guyot-Sionnest P. Interband and Intraband Optical Studies of PbSe Colloidal Quantum Dots. J Phys Chem B. 2002; 106:10634–10640.
7. Bakueva L, Gorelikov I, Musikhin S, Zhao XS, Sargent EH, Kumacheva E. PbS Quantum Dots with Stable Efficient Luminescence in the Near-IR Spectral Range. Adv Mater. 2004; 16:926–929.
8. Harrison MT, Kershaw SV, Burt MG, Eychmuller A, Weller H, Rogach AL. Wet Chemical Synthesis and Spectroscopic Study of CdHgTe Nanocrystals with Strong Near-Infrared Luminescence. Mater Sci Eng B. 2000; 69:355–360.
9. Zrazhevskiy P, Senawb M, Gao X. Designing Multifunctional Quantum Dots for Bioimaging, Detection, and Drug Delivery. Chem Soc Rev. 2010; 39:4326–4354. [PubMed: 20697629]
10. Leeuw TK, Reith RM, Simonette RA, Harden ME, Cherukuri P, Tsyboulski DA, Beckingham KM, Weisman RB. Carbon Nanotubes as Photoacoustic Molecular Imaging Agents in Living Mice. Nat Nanotech. 2008; 3:557–562.
11. Welsher K, Liu Z, Daranciang D, Dai H. Selective Probing and Imaging of Cells with Single Walled Carbon Nanotubes as Near-Infrared Fluorescent molecules. Nano Lett. 2008; 8:586–590. [PubMed: 18197719]
12. Chen Z, Tabakman SM, Goodwin AP, Kattah MG, Daranciang D, Wang XR, Zhang GY, Li XL, Liu Z, Utz PJK, et al. Protein Microarrays with Carbon Nanotubes as Multicolor Raman Labels. Nat Biotech. 2008; 26:1285–1292.
13. Kam NWS, O'Connell M, Wisdom JA, Dai H. Carbon Nanotubes as Multifunctional Biological Transporters and Near-Infrared Agents for Selective Cancer Cell Destruction. PNAS. 2005; 102:11600–11605. [PubMed: 16087878]

14. Hong G, Tabakman SM, Welsher K, Chen Z, Robinson JT, Wang H, Zhang B, Dai H. Near-Infrared-Fluorescence-Enhanced Molecular Imaging of Live Cells on Gold Substrates. Angew Chem Int Ed. 2011; 50:4644–4647.
15. Robinson JT, Welsher K, Tabakman SM, Sherlock SP, Wang H, Luong R, Dai H. High Performance in vivo Near-IR (>1 μm) Imaging Photothermal Cancer Therapy with Carbon Nanotubes. Nano Res. 2010; 3:779–793. [PubMed: 21804931]
16. Hong G, Tabakman SM, Welsher K, Wang H, Wang X, Dai H. Metal-Enhanced Fluorescence of Carbon Nanotubes. J Am Chem Soc. 2010; 132:15920–15923. [PubMed: 20979398]
17. De La Zerda A, Liu Z, Bodapati S, Teed R, Vaithilingam S, Khuri-Yakub BT, Chen X, Dai HJ, Gambhir SS. Ultrahigh Sensitivity Carbon Nanotube Agents for Photoacoustic Molecular Imaging in Living Mice. Nano Lett. 2010; 10:2168–2172. [PubMed: 20499887]
18. O'Connell MJ, Bachilo SM, Huffman CB, Moore VC, Strano MS, Haroz EH, Rialon KL, Boul PJ, Noon WH, Kittrell C, et al. Band Gap Fluorescence from Individual Single-Walled Carbon Nanotubes. Science. 2002; 297:593–596. [PubMed: 12142535]
19. Crochet J, Clemens M, Hertel T. Quantum Yield Heterogeneities of Aqueous Single-Wall Carbon Nanotube Suspensions. J Am Chem Soc. 2007; 129:8058–8059. [PubMed: 17552526]
20. Du Y, Xu B, Fu T, Cai M, Li F, Zhang Y, Wang Q. Near-Infrared Photoluminescent Ag_2S Quantum Dots from a Single Source Precursor. J Am Chem Soc. 2010; 132:1470–1471. [PubMed: 20078056]
21. Shen S, Zhang YJ, Peng L, Du Y, Wang Q. Matchstick-Shaped Ag_2S-ZnS Heteronanostructures Preserving both UV/Blue and Near-Infrared Photoluminescence. Angew Chem Int Ed. 2011; 50:7115–7118.
22. Murphy JE, Beard MC, Norman AG, Ahrenkiel SP, Johnson JC, Yu P, Mićić OI, Ellingson RJ, Nozik AJ. PbTe Colloidal Nanocrystals: Synthesis, Characterization, and Multiple Exciton Generation. J Am Chem Soc. 2006; 128:3241–3247. [PubMed: 16522105]
23. Liu Z, Tabakman SM, Chen Z, Dai H. Preparation of Carbon Nanotube Bioconjugates for Biomedical Applications. Nat Protoc. 2009; 4:1372–1382. [PubMed: 19730421]
24. Kam NWS, Liu Z, Dai H. Carbon Nanotubes as Intracellular Transporters for Proteins and DNA: an Investigation of the Uptake Mechanism and Pathway. Angew Chem Int Ed. 2005; 44:1–6.
25. White JG, Krivit W. An Ultrastructural Basis for the Shape Changes Induced in Platelets by Chilling. Blood. 1967; 30:625–635. [PubMed: 6073858]
26. Andreyev AY, Kushnareva YE, Starkov AA. Mitochondrial Metabolism of Reactive Oxygen Species. Biochemistry. 2005; 70:200–214. [PubMed: 15807660]
27. AshaRani PV, Mun GLK, Hande MP, Valiyaveettil S. Cytotoxicity and Genotoxicity of Silver Nanoparticles in Human Cells. ACS Nano. 2009; 3:279–290. [PubMed: 19236062]
28. Olive PL, Banath JP. The Comet Assay: a Method to Measure DNA Damage in Individual Cells. Nat Protoc. 2006; 1:23–29. [PubMed: 17406208]
29. Li F, Li K, Cui ZQ, Zhang ZP, Wei HP, Gao D, Deng JY, Zhang XE. Viral Coat Proteins as Flexible Nano Building Blocks for Nanoparticle Encapsulation. Small. 2010; 6:2301–2308. [PubMed: 20842665]
30. Yang H, Rivera Z, Jube S, Nasu M, Bertino P, Goparaju C, Franzoso G, Lotze MT, Krausz T, Pass HI, et al. Programmed Necrosis Induced by Asbestos in Human Mesothelial Cells Causes High-Mobility Group Box 1 Protein Release and Resultant Inflammation. PNAS. 2010; 107:12611–12616. [PubMed: 20616036]

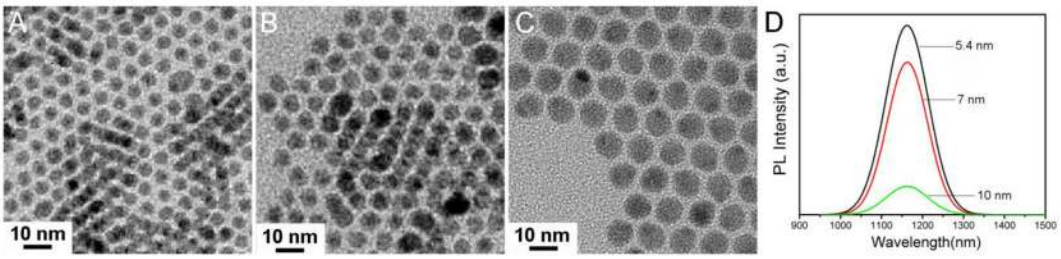

Figure 1.
TEM images (A–C) and PL spectra (D) of three DT-Ag_2S QDs with different sizes. A: 5.4 nm; B: 7 nm; C: 10 nm.

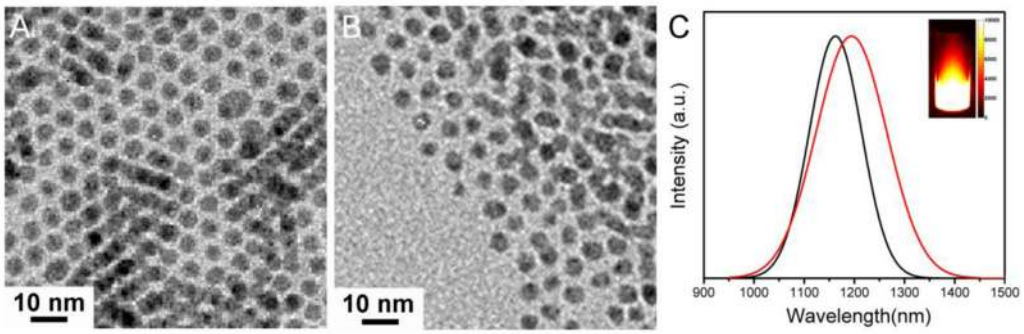

Figure 2.
TEM images of DT-Ag_2S QDs (A) and DHLA-Ag_2S QDs (B), and their NIR PL spectra (C) (black line: DT-Ag_2S QDs; red line: DHLA-Ag_2S QDs). Inset shows a photoluminescence image of DHLA-Ag_2S QDs suspension under an 808 nm excitation.

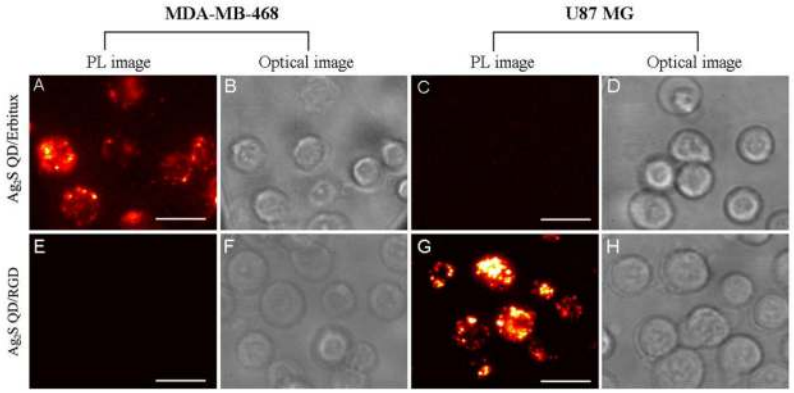

Figure 3.

In vitro targeted cellular imaging. NIR-II PL images (1100 – 1700 nm) of MDA-MB-468 and U87 MG cells treated with DHLA-Ag_2S QD/Erbitux conjugates (A, C) and their corresponding optical images (B, D); NIR-II PL images (1100 – 1700 nm) of MDA-MB-468 and U87 MG cells treated DHLA-Ag_2S QD/RGD conjugates (E, G) and their corresponding optical images (F, H). Erbitux ligand specifically binds to MDA-MB-468 cells and RGD peptide ligand specifically binds to U87 MG cells. NIR-II images were taken with exposure time of 300 ms and optical images with exposure time of 2 ms. Scale bars are 25 μm.

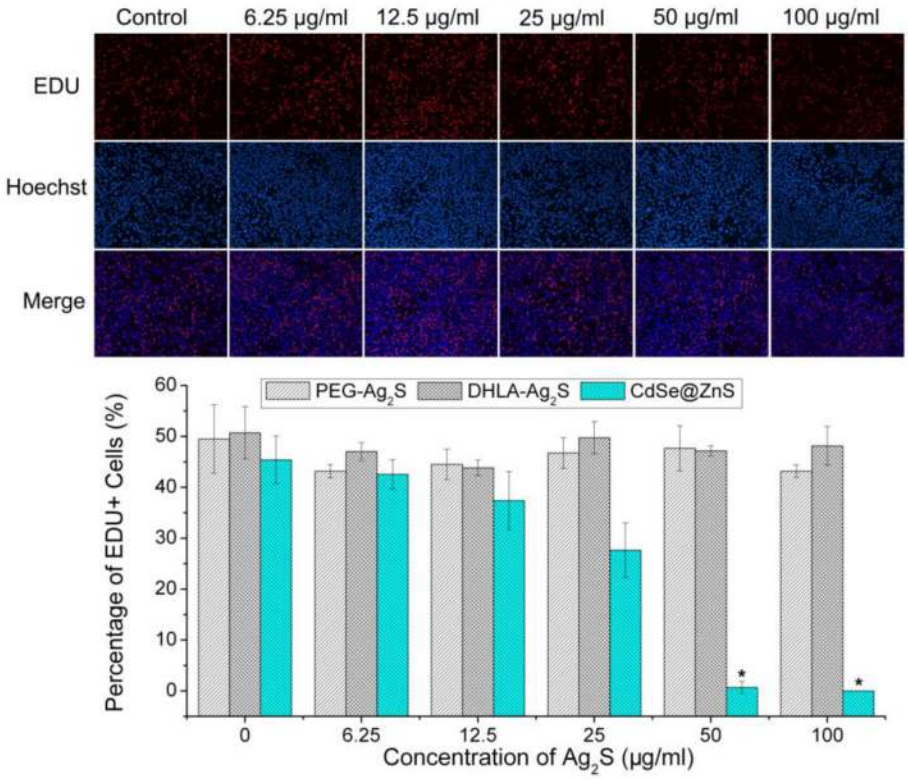

Figure 4.

Effect of DHLA-Ag_2S QDs on the L929 cell proliferation after 72 h treatment. Top: Representative images of EdU assay of Hoechst stained cells and EdU add-in cells incubated with different concentrations of DHLA-Ag_2S QDs; Bottom: Quantification of EdU-positive proliferating cells treatment were counted by collecting more than 200 cells. PEG-DHLA-Ag_2S QDs and MPA-capped CdSe@ZnS QDs were chosen as references under the same conditions (*: $P < 0.05$).

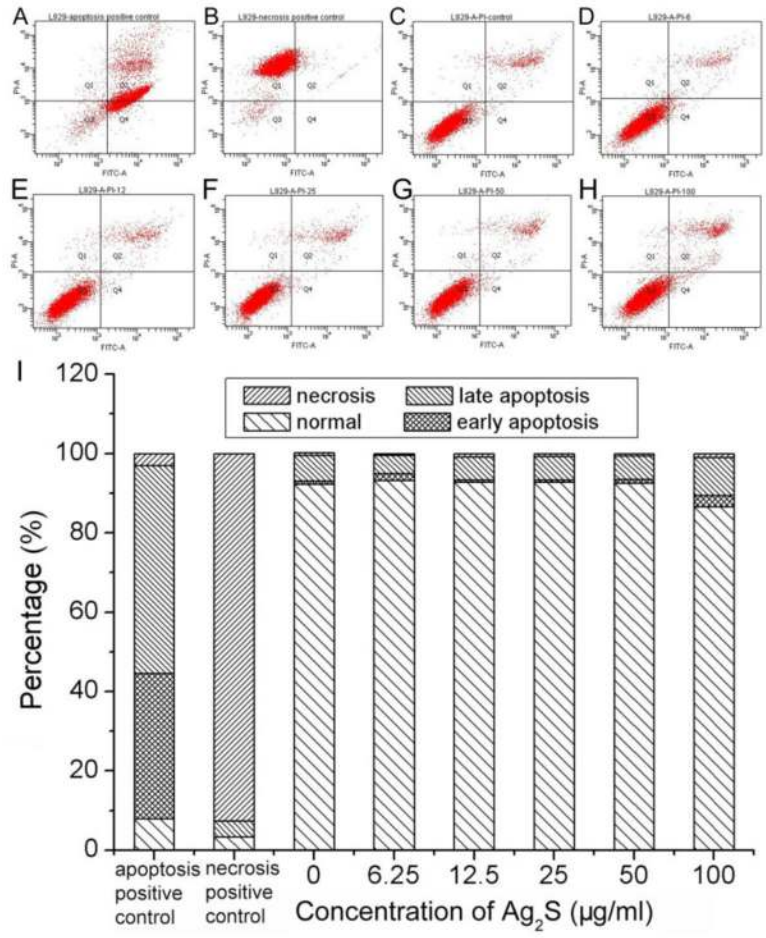

Figure 5.

Apoptosis and necrosis of L929 cells caused by DHLA-Ag_2S QDs after 72 h treatment. A: apoptosis positive control of acinomycin D at a concentration of 0.1 μM; B: necrosis positive control of H_2O_2 at a concentration of 1 mM; C–H: FACS plots with Ag_2S QD concentrations at 0, 6.25, 12.5, 25, 50 and 100 μg/mL, respectively. I: quantitative flow cytometry results.

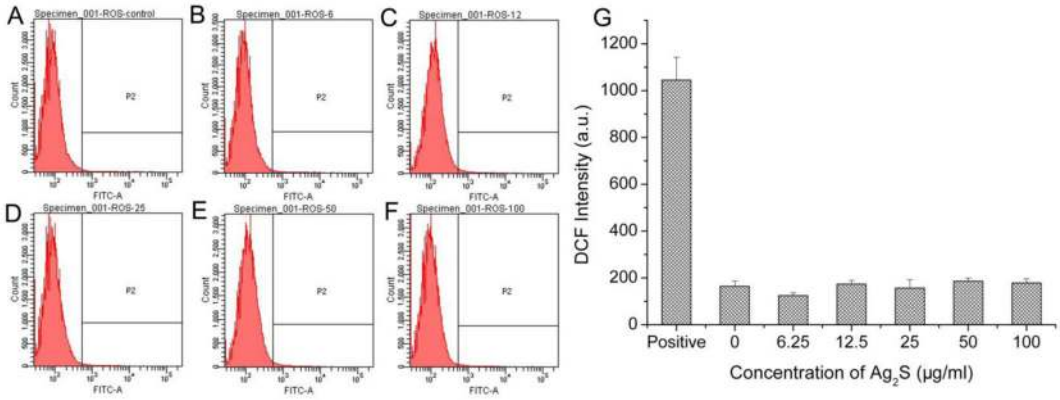

Figure 6.

ROS induced by DHLA-Ag_2S QDs after 72 h treatment. A–F: FACS plots with Ag_2S QD concentrations at 0, 6.25, 12.5, 25, 50 and 100 μg/mL, respectively. G: Quantitative flow cytometry results. P2 indicates the cell population that produces ROS. Positive stands for the positive control of Rosup at a concentration of 50 μg/mL.

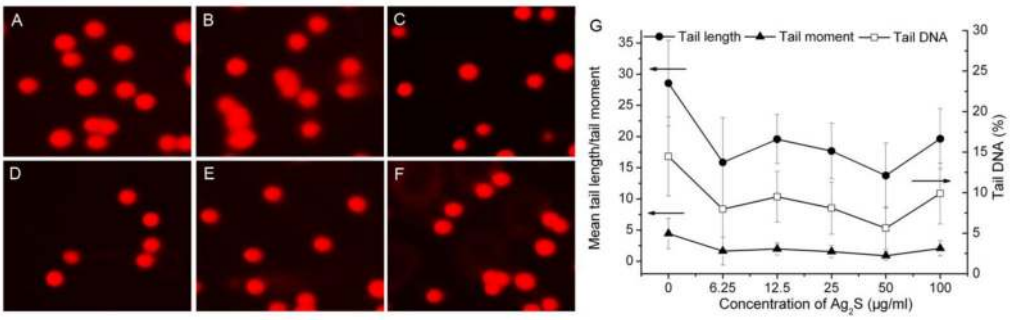

Figure 7.

Effect of DHLA-Ag_2S QDs on DNA damage in L929 cells with respect to tail length/tail moment and DNA% in tail after 72 h treatment. A–F: Comet assay images with Ag_2S QD concentrations at 0, 6.25, 12.5, 25, 50 and 100 μg/mL, respectively. G: comet assay results.